Phase Transformation Behavior of Cu-10Ni-3Al-0.8Si alloy

Leinuo Shen [a], Zhou Li [a,*], Yuyuan Zhao [b], Yang Wang [c], Qiyi Dong [a, d], Mengying Wang [a]

a School of Materials Science and Engineering, Central South University, Changsha, 410083, China

b School of Engineering, University of Liverpool, Liverpool, L69 3GH, United Kingdom

c School of Mechanical Engineering, Hefei University of Technology, Xuancheng Campus, HeFei, 242000, China

d Key Laboratory of Nonferrous Metal Materials Science and Engineering, Ministry of Education, Changsha, 410083, China

* Corresponding author. E-mail address: lizhou6931@163.com (Z. Li).

Highlights

- Modulated structure, ordering formed; then Ni_3Al, δ-Ni_2Si nucleated at 450 °C.
- Micro-twins formed after aged at 450 °C for 30 s and improved the strength.
- Increase temperature, precipitation accelerated, discontinuous phase formed.
- Cellular decomposition occurred and Ni_3Al dissolved at 750 °C.

Keywords: Alloys, Precipitation, Electron microscopy, Microstructure

Abstract

Microstructure evolution of solution treated Cu-10Ni-3Al-0.8Si alloy aged at different temperatures was investigated and different transformation products were observed: modulated structure resulting from spinodal decomposition, $L1_2$ ordering of matrix, continuous Ni_3Al precipitates, continuous δ-Ni_2Si precipitates and discontinuous precipitates. Modulated structure, $L1_2$ ordering of matrix and micro-twins formed initially at 450 °C, while continuous Ni_3Al and δ-Ni_2Si particles precipitated soon. Increasing temperature led to the formation of discontinuous precipitates, dissolution of Ni_3Al and cellular decomposition. The alloy showed excellent over-aging resistance at 450 °C because the Ni_3Al and δ-Ni_2Si precipitates grew very slowly and the addition of silicon hindered the precipitation of the coarsening NiAl phase.

1. Introduction

Cu-Be alloy has been widely used as elastic springs, bearings and contact switches in electric industry, due to its excellent comprehensive properties with ultra-high strength of about 1250 MPa and electrical conductivity of 20% IACS when solution treated and aged at 320 °C for 3 h [1,2]. However, the stress relax resistant rate of Cu-Be alloy increases over 20% when held at 150 °C for 100 h, which limits its many applications [3]. The toxic beryllium element evaporates during casting and mechanical processing, which would and could cause pneumonia and cancer. Therefore, Cu-Ni-Sn, Cu-Ti and Cu-Ni-Al alloys have been developed to replace Cu-Be alloy in recent years [4-6]. For elastic copper alloys, increasing the electrical conductivity can significantly increase the efficiency of the signal transmission and reduce the temperature rise, thus can extend the life of the device. In order to improve electrical conductivity and grantee ultra-high strength of environment friendly copper alloys, the Cu-10Ni-3Al-0.8Si alloy with tensile strength of 1180 MPa and electrical conductivity of 18.1% IACS has been designed [7].

The ultra-high strength and good electrical conductivity of Cu-Ni-Al alloys are attributable to the precipitation hardening effect during aging [8]. However, the sequences of precipitation and the structures of precipitates of these alloys are still under debate. Hiroshi et al. [9] found that only spherical coherent Ni3Al precipitates with $L1_2$ ordered structure formed in the Cu-5Ni-2.5Al alloy during aging at 500 °C. Cho et al. [10] found that except for coherent Ni_3Al precipitates, discontinuous NiAl also precipitated in the Cu-7Ni-3Al alloy aged at 500 °C, and the hardness and strength of the alloy decreased significantly when large NiAl phase precipitated. The work of Masamich et al. [11] revealed that the super-saturated solid solution in the Cu-30Ni-3Al alloy decomposed into modulated structure at the initial stage of aging and then developed to the equilibrium phase with the composition ranging from $(Ni_{0.67}Cu_{0.33})Al$ to $(Ni_{0.85}Cu_{0.15})Al$, but satellite spots of spinodal decomposition were not observed. Alexander [12] also studied the precipitation of the Cu-30Ni-5Al alloy at 500 °C and indicated that both Ni_3Al and coarse NiAl phases precipitated and the precipitation of large NiAl precipitates deteriorated the properties of the alloy. Addition of silicon in Cu-Ni based alloys results in the precipitation of several types of nickel-silicon intermetallic compounds, such as δ-Ni_2Si, β-Ni_3Si and NiSi [13,14]. Amin et al. [15] reported that the tensile strength and yield strength of Cu-4.6Ni-4Al-1Si alloy increased to 1000 MPa and 950 MPa, respectively, due to the formation of fine precipitates (Ni_3Si, Ni_2Si, Ni_2Al). However, the influence of silicon on microstructure and precipitation sequence of solution treated Cu-Ni-Al-Si alloys has not been fully studied.

This study investigates the species of precipitates and precipitation sequence in the Cu-10Ni-3Al-0.8Si alloy during isothermal aging at different temperatures, studies the influence of microstructure on mechanical properties and electrical conductivity of the alloy, and discusses the mechanisms of phase transformation.

2. Experimental procedure

The Cu-10Ni-3Al-0.8Si alloy (wt.%) was prepared with pure Cu, Ni, Al and Si by conventional casting in a medium-frequency induction furnace. After surface defects were removed, the cast ingot was hot rolled by 60% at 920 °C and then cold rolled by 60%. The cold-rolled plate was solid-solution treated at 950 °C for 4 h, followed by water quenching, and then was isothermally aged at a temperature range from 400 °C to 750 °C with a step of 50 °C.

Vickers hardness was measured by a Vickers hardness tester under a load of 3 kg and a holding time of 10 s. Relative electrical conductivity was measured at 20 °C by a D60 K digital metal electrical conductivity tester. The transmission electron microscopy (TEM), selected area diffraction pattern (SADP) and high resolution transmission electron microscopy (HRTEM) observations were performed on a JEM-2100F microscopy, with the operation voltage of 200 kV. The specimens for TEM observations were mechanically reduced to 0.06 mm and then electron-polished by the standard twin-jet electro-polishing method in a 3:1 methanol-nitric acid solution between -20 °C and -30 °C.

3. Results and discussion

3.1. Mechanical and electrical properties

Fig. 1a shows the variation of Vickers hardness of the solution treated Cu-10Ni-3Al-0.8Si alloy isothermally aged at different temperatures. When the aging temperature was below 500 °C, the Vickers hardness increased steadily with aging time during the whole stage of aging. When the solution treated alloy was isothermally aged at 500 °C or above, the Vickers hardness increased rapidly at the initial stage of aging and then decreased after reaching the peak values. The value of peak hardness and the time to reach the peak hardness decreased with aging temperature.

The electrical conductivity of the solution treated alloy increased considerably with aging time and temperature, when the aging temperature was below 600 °C. Further increasing aging temperature to over 600 °C, electrical conductivity of the alloy aged for over 8 h decreased with aging temperature, indicated the decrease of volume fraction of precipitates (Fig. 1b).

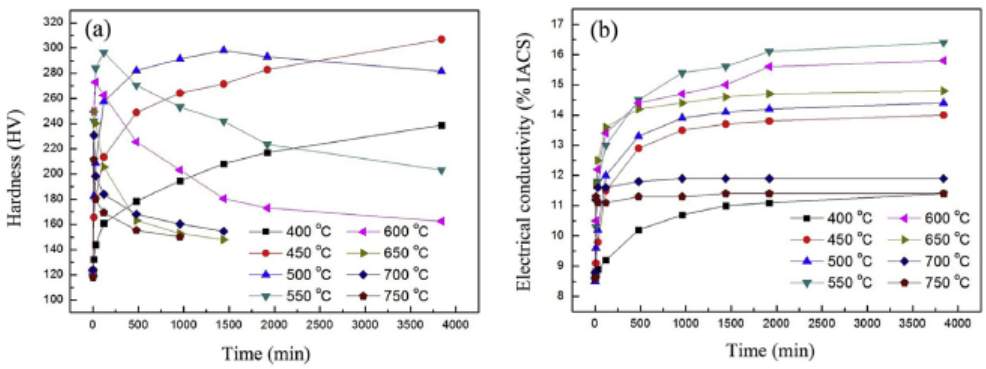

Fig. 1. Effects of aging temperature and time on properties of Cu-10Ni-3Al-0.8Si alloy (a) Vickers hardness of solution treated alloy; (b) electrical conductivity of solution treated alloy.

3.2. Microstructure at 450 °C

The TEM micrographs of the alloy aged at 450 °C for 30 s are shown in Fig. 2a, b and c. The bright field micrograph (Fig. 2a) showed that modulated structure with bright-and-dark contrast formed in the matrix. The satellite spots with directions along $[100]_{Cu}$ and $[0\bar{1}0]_{Cu}$ were observed in Fig. 2b. Both indicated that spinodal decomposition occurred as the alloy aged at 450 °C for 30 s. The SADP (Fig. 2b) indicated that $L1_2$ ordering occurred in the matrix. It is especially interesting that micro-twins was observed in the solution treated alloy aged at 450 °C for 30 s (Fig. 2c). This has not been reported previously in bulk copper alloys, although Wang et al. [16] reported the formation of micro-

twins in sputtered Cu films. These micro-twins resulted from the release of quenching stress and could significantly improve the strength and hardness of the alloy because the twin boundaries can hinder the movement of dislocations.

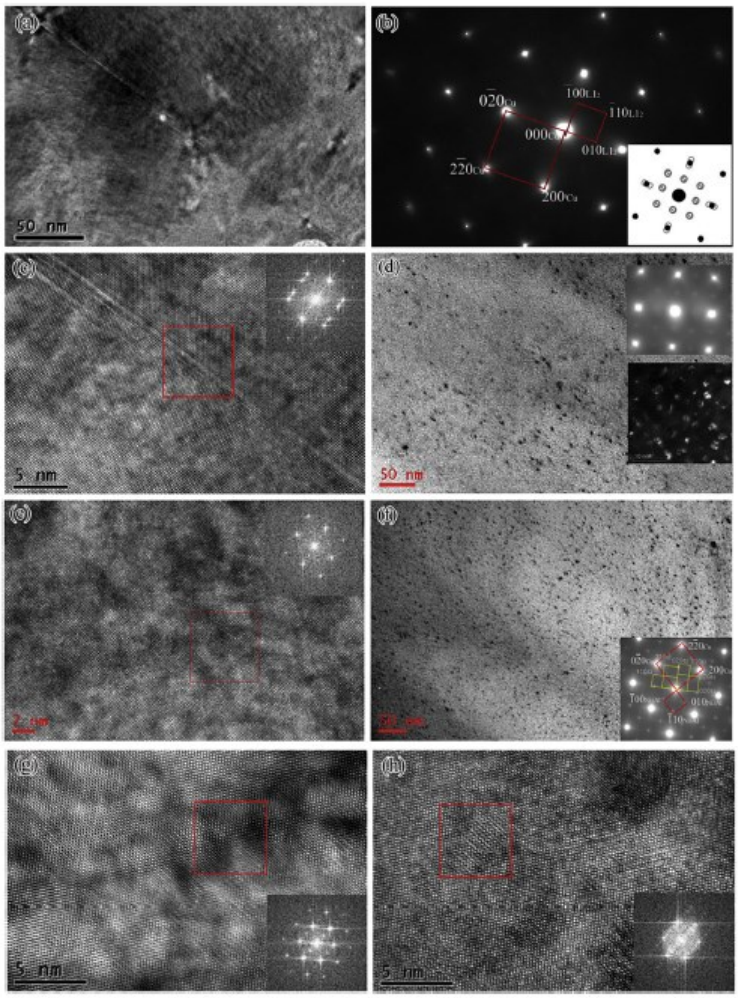

Fig. 2. Micrographs of the alloy aged at 450 °C for 30 s, 1 min and 5 min (a) bright field micrograph for 30 s; (b) SADP with beam direction along [100]Cu for 30 s; (c) HRTEM for 30 s; (d) bright-field, SADP and dark field micrograph for 1 min; (e) HRTEM of Ni_3Al for 1 min; (f) bright-field micrograph and SADP for 5 min; (g) HRTEM of Ni_3Al for 5 min; (h) HRTEM of Ni_2Si for 5 min.

Fig. 2d and e shows the TEM micrographs of the alloy aged at 450 °C for 1 min. A high density of nano-scale Ni_3Al particles with $L1_2$ ordered structure precipitated in the matrix (Fig. 2d). The SADP, dark filed and HRTEM micrograph showed that these Ni_3Al precipitates with particle size of about 3 nm were coherent with the matrix (Fig. 2d and e). The orientation relationships between the Ni_3Al precipitates and the copper matrix were: $[001]_{Cu}//[001]_{Ni3Al}$, $(110)_{Cu}//(110)_{Ni3Al}$, and $(1\bar{1}0)_{Cu}//(1\bar{1}0)_{Ni3Al}$.

The TEM micrographs of the alloy aged at 450 °C for 5 min are shown in Fig. 2f, g and h. The bright field micrograph and the corresponding SADP (Fig. 2f) indicated that both Ni_3Al precipitates with $L1_2$ ordered structure and δ-Ni_2Si precipitates precipitated in the matrix. The HRTEM micrographs of

Ni_3Al (Fig. 2g) and δ-Ni_2Si (Fig. 2h) showed that the precipitates were coherent with the matrix with particle size of about 3 nm and 4 nm, respectively. The orientation relationships between the δ-Ni_2Si precipitates and the copper matrix were: $[001]_{Cu}//[001]_{\delta}$, $(110)_{Cu}//(110)_{\delta}$, and $(1\bar{1}0)_{Cu}//(100)_{Ni3Al}$.

The TEM micrographs of the alloy aged at 450 °C for 64 h are shown in Fig. 3. Both Ni_3Al particles with zero-contrast lines and δ-Ni_2Si particles without zero-contrast lines precipitated in the grains (Fig. 3a). However, precipitates were not observed at the grain boundaries (Fig. 3b), indicating that only continuous precipitation occurred when aged at 450 °C for 64 h.

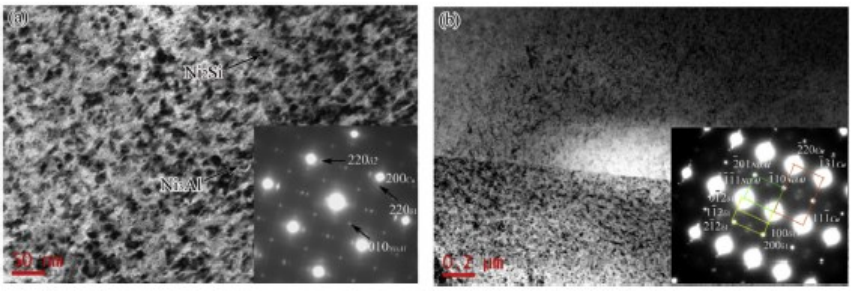

Fig. 3. Micrographs of the alloy aged at 450 °C for 64 h (a) bright-field micrograph and SADP in the grain; (b) bright-field micrograph and SADP at grain boundary.

3.3. Microstructure at 550 °C

The TEM micrographs of the alloy aged at 550 °C for 30 s are shown in Fig. 4. No spinodal decomposition occurred, but a large number of nano-scale Ni_3Al precipitates were found in the matrix (Fig. 4a). The Ni_3Al precipitates were only about 2 nm and completely coherent with the copper matrix (Fig. 4b).

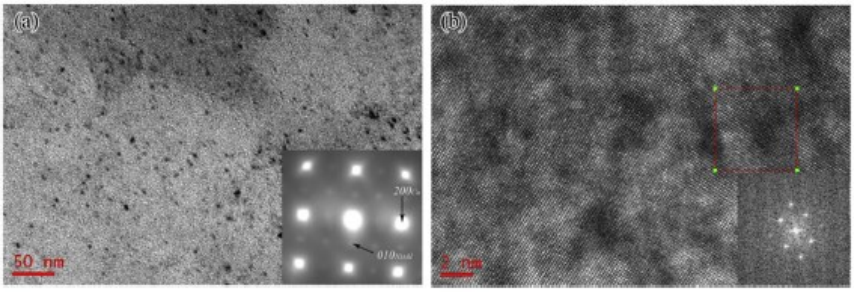

Fig. 4. Micrographs of the alloy aged at 550 °C for 30 s (a) bright-field micrograph and SADP; (b) HRTEM of Ni3Al.

The bright field TEM micrographs of the alloy aged at 550 °C for 1 min are shown in Fig. 5a and b. A great number of Ni_3Al and δ-Ni_2Si precipitates precipitated in the matrix and discontinuous precipitation occurred at the grain boundary (Fig. 5a and b). The δ-Ni_2Si precipitates had two variants mutually perpendicular to each other and the particle sizes of the δ-Ni_2Si and Ni_3Al precipitates were about 5 nm and 4 nm, respectively (Fig. 5c). Both precipitates were coherent with the matrix.

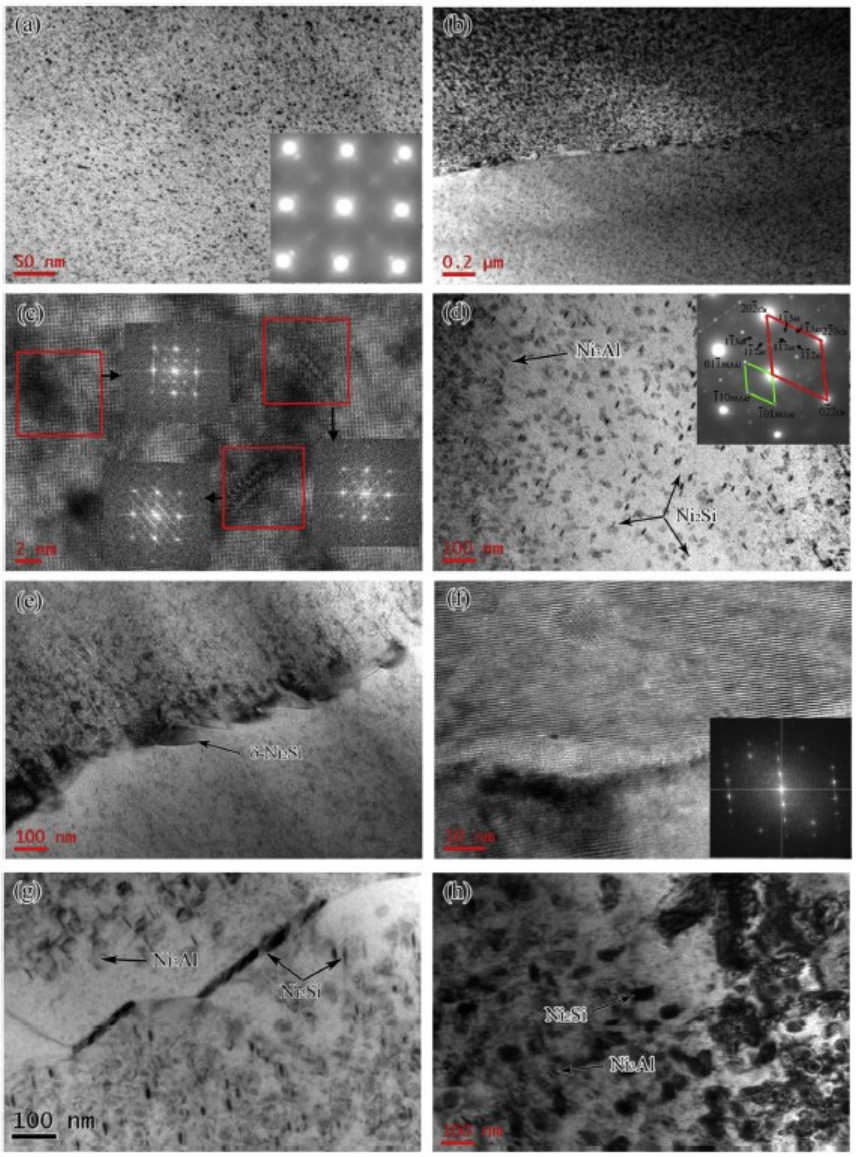

Fig. 5. Micrographs of the alloy aged at 550 °C for different times (a) bright-field micrograph and SADP in the grain for 1 min; (b) bright-field micrograph at grain boundary for 1 min; (c) HRTEM of Ni3Al and δ-Ni_2Si for 1 min; (d) bright field micrograph and SADP in the grain for 30 min; (e) bright field micrograph at the grain boundary for 30 min; (f) HRTEM of δ-Ni_2Si at the grain boundary for 30 min; (g) bright-field micrograph for 120 min; (h) bright-field micrograph for 960 min.

When the alloy was aged for 30 min, δ-Ni_2Si precipitates with three variants (60° with each other), and Ni_3Al precipitates with zero-contrast lines, precipitated in the matrix, and the particle sizes of these precipitates were about 15 nm and 8 nm, respectively (Fig. 5d). Large, discontinuous δ-Ni_2Si particles with sizes of about 80 nm precipitated at the grain boundaries (Fig. 5e and f). When aging time prolonged to 120 min, continuous Ni_3Al and δ-Ni_2Si precipitates grew up to 15 nm and 25 nm, respectively; while discontinuous precipitates at the grain boundary were over 120 nm (Fig. 5g). Further increasing aging time to 960 min, Ni_3Al and δ-Ni_2Si particles significantly coarsened up to 50 nm and 60 nm, respectively (Fig. 5h).

3.4. Microstructure at 650 °C

Fig. 6 shows the TEM micrographs of the alloy aged at 650 °C for different times. When the alloy was aged for 30 s, both Ni_3Al and δ-Ni_2Si with particle size of about 10 nm, precipitated in the matrix (Fig. 6a). Discontinuous precipitation was observed at the grain boundaries (Fig. 6b). The corresponding HRTEM micrograph of the discontinuous precipitates indicated that the precipitates were δ-Ni_2Si with particle size of over 200 nm (Fig. 6c). When the aging time was prolonged to 15 min, the Ni_3Al precipitates with zero-contrast lines grew up to about 30 nm and the δ-Ni_2Si precipitates with Morie fringe coarsened to about 50 nm (Fig. 6d).

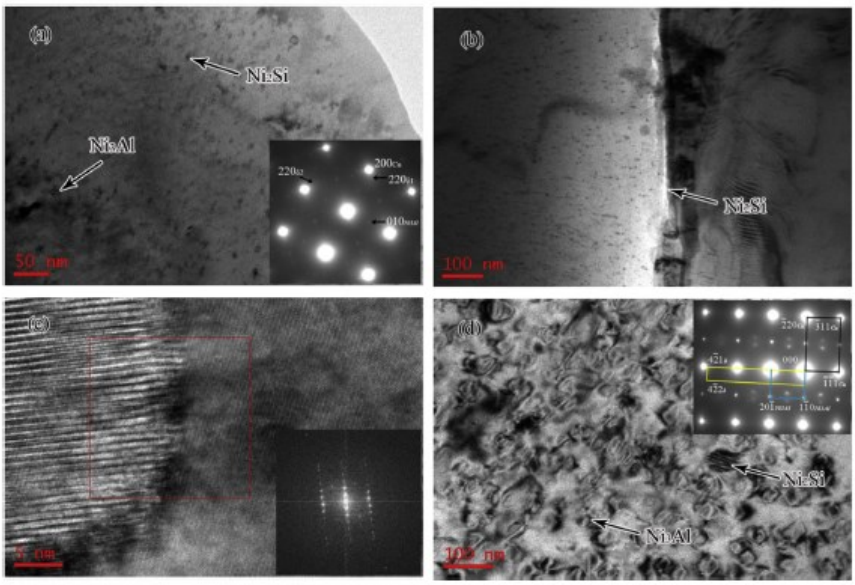

Fig. 6. Micrographs of the alloy aged at 650 °C for different times. (a) bright field micrograph and SADP of matrix for 30 s; (b) bright field micrograph along the grain boundary for 30 s; (c) HRTEM of δ-Ni_2Si at the grain boundary for 30 s; (d) bright field micrograph and SADP in the matrix for 15 min.

3.5. Microstructure at 750 °C

Fig. 7 shows TEM micrographs of the alloy aged at 750 °C for various times. Continuous δ-Ni_2Si and Ni_3Al precipitates with particle size of 8 nm precipitated in the alloy after aging for 30 s (Fig. 7a). When the aging time increased to 15 min, the δ-Ni_2Si precipitates coarsened up to 80 nm, and cellular structure and discontinuous precipitation were observed (Fig. 7b and c). Except for the diffraction of matrix, only the diffraction spots of δ-Ni_2Si were detected in the corresponding SADP, indicating that Ni_3Al had dissolved into the matrix.

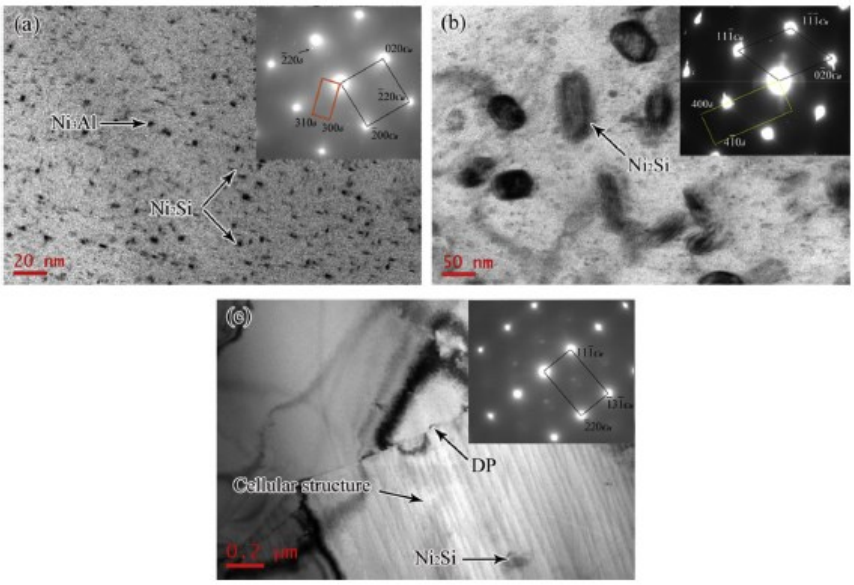

Fig. 7. Micrographs of the alloy aged at 750 °C for different times. (a) bright field micrograph and SADP for 30 s; (b) bright field micrograph and SADP of matrix for 15 min; (c) bright field micrograph and SADP of cellular structure for 15 min.

3.6. Formation of precipitates

The experimental results presented above indicated that the phase transformation sequence of the solution treated Cu-10Ni-3Al-0.8Si alloy aged at 450 °C was: modulated structure resulting from spinodal decomposition and $L1_2$ ordering of the matrix occurred, while continuous Ni_3Al precipitates with $L1_2$ ordered structure and δ-Ni_2Si phase precipitated as aging time prolonged. When aging temperature increased to 550 °C, continuous Ni_3Al precipitates formed at 30 s, followed by continuous δ-Ni_2Si precipitation in the grains and discontinuous δ-Ni_2Si precipitation at the grain boundaries at 1 min. When the alloy aged at 650 °C for 30 s, continuous Ni_3Al and δ-Ni_2Si precipitated and discontinuous precipitation occurred. Further increasing aging temperature to 750 °C, continuous Ni_3Al and δ-Ni_2Si precipitated at 30 s, while metastable Ni_3Al dissolved and cellular decomposition occurred after aging for 15 min.

The precipitation behaviors of the solution treated Cu-10Ni-3Al-0.8Si alloy can be explained by the classical nucleation theory of phase transformation. The driving force for the nucleation of precipitates is the change of Gibbs free energy, and the formation of precipitates with low formation enthalpies is favored [17]. The formation enthalpies of precipitates can be calculated according to Miedema model [18,19]:

$$\Delta H_{ab} = \frac{f_{ab}\{x_a[1+\mu_a x_b(\phi_a-\phi_b)]x_b[1+\mu_b x_a(\phi_b-\phi_a)]\}}{\left\{x_a V_a^{\frac{2}{3}}[1+\mu_a x_b(\phi_a-\phi_b)]x_b V_b^{\frac{2}{3}}[1+\mu_b x_a(\phi_b-\phi_a)]\right\}} \quad (1)$$

with f_{ab} being:

$$f_{ab} = \frac{2pV_a^{\frac{2}{3}}V_b^{\frac{2}{3}}\left\{\frac{q}{p}\left[\left(n_{ws}^{\frac{1}{3}}\right)_a - \left(n_{ws}^{\frac{1}{3}}\right)_b\right]^2 - (\phi_a - \phi_b)^2 - \alpha\left(\frac{r}{p}\right)\right\}}{\left[\frac{1}{\left(n_{ws}^{\frac{1}{3}}\right)_a} + \frac{1}{\left(n_{ws}^{\frac{1}{3}}\right)_b}\right]} \quad (2)$$

where, ΔH_{ab} is the formation enthalpy of the precipitate; f_{ab} is the enclosure extent of atom b around atom a; α, μ, p, q, and r are empirical constants (α is 1 for Ni, Al and Si; μ is 0.04 for Ni, Al and Si; q/p is 9.4 for Ni, Al and Si; r/p is 1, 1.9 and 2.1 for Ni, Al and Si, respectively); f_a and f_b are the electronegativity of atoms a and b (the electronegativity of Ni, Al and Si is 5.20, 4.20 and 4.70, respectively); V_a and V_b are the molar volumes of atoms a and b (the molar volumes of Ni, Al and Si is 3.50, 4.64 and 4.20, respectively); and $n_{ws}^{1/3}$ is the Wigner-Seitz boundary electron concentration of the pure metal ($n_{ws}^{1/3}$ of Ni, Al, and Si is 1.75, 1.39 and 1.50, respectively) [18,19].

Fig. 8 shows the formation enthalpies of the compounds that might precipitates in the Cu-10Ni-3Al-0.8Si alloy, calculated by Eqs. (1) and (2). The formation enthalpies of Ni_3Al, δ-Ni_2Si and NiSi phases are negative, while the NiAl phase shows the lowest formation enthalpy. The effect of entropy change can be ignored as it is unlikely to reverse the large difference between the lowest and the nearest formation enthalpies [20]. The negative formation enthalpies indicate that all these phases are liable to precipitate from the super saturated solid solution. The NiAl phase with the lowest formation enthalpy is the most stable phase in the Cu-10Ni-3Al-0.8Si alloy at any temperature and its nucleation should have been favored. However, addition of Si inhibited the precipitation of NiAl in the Cu-10Ni-3Al-0.8Si alloy. Only Ni_3Al and δ-Ni_2Si precipitated during aging.

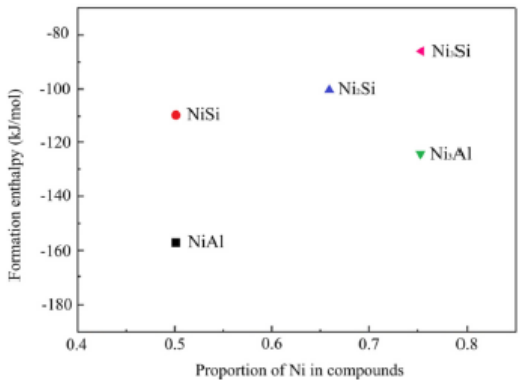

Fig. 8. Formation enthalpies of various compounds.

In general, the interfacial energy and elastic strain energy between the precipitates and the matrix also have influence on the formation of precipitates. Assuming that the precipitates were coherent with copper matrix as nucleated, elastic strain energy would be much larger than the interface strain energy for all the precipitates, thus the formation of precipitate with low elastic strain energy would be favored [21]. The nucleation and growth of these phases mainly depend on the elastic strain energy. Assuming that the precipitates formed at the initial stage of aging are coherent or semi-

coherent spherical particles, which have purely dilatational misfit strains, the elastic strain energy of the precipitates can be calculated by [22]:

$$E = \frac{6A(1+\nu)}{\{A(1+\nu)+2(1-2\nu)\}} G\varepsilon^2 \quad (3)$$

where, E is the elastic strain energy of the precipitates, *A* is the elastic constant of the precipitates [23], ν is the Poisson's ratio (0.34 for Cu), ε is the elastic strain between the precipitates and the matrix [7], *G* is the sheer modulus of matrix (45.5 GPa for Cu).

Table 1 shows the elastic strain energy of all possible compounds in the Cu-10Ni-3Al-0.8Si alloy. Although the NiAl, β-Ni_3Si and NiSi phases have negative formation enthalpies, their high elastic strain energies would hinder the nucleation of these phases. Therefore, δ-Ni_2Si and Ni_3Al precipitates would form because of their low elastic strain energies.

Table 1
Calculated elastic strain energy of compounds.

Compounds	NiAl	Ni_3Al	NiSi	δ-Ni_2Si	β-Ni_3Si
E (kJ/m^3)	1082.75	327.92	6633.66	92.34	2073.43

Although Ni_3Al has larger elastic strain energy than δ-Ni_2Si, the precipitation of Ni_3Al phase with $L1_2$ ordering structure occurred at the very early stage of aging. This is because $L1_2$ ordering of matrix occurred at 450 °C for 30 s, while structure of Ni_3Al is similar with that of ordering matrix. In other words, the nucleation of Ni_3Al involves only localizes atomic rearrangement while the nucleation of δ-Ni_2Si requires longer range atomic diffusion [24]. Therefore, the energy barrier for the nucleation of Ni_3Al is much lower than that for Ni_2Si, and Ni_3Al precipitates earlier than Ni_2Si.

It has been reported that Ni_3Al precipitates dissolved and stable NiAl precipitates nucleated at the grain boundaries of recrystallized grains at the later stage of aging in the Cu-10Ni-3Al alloy [25]. In our experiments, we observed that the metastable Ni_3Al particles in the solution treated Cu-10Ni-3Al-0.8Si alloy dissolved after being aged at 750 °C for 15 min, consistent with the fact that Ni_3Al has a solid solution temperature of about 780 °C [12]. However, large NiAl precipitates were not observed. This is attributable to the addition of silicon in the Cu-10Ni-3Al-0.8Si alloy. The elastic strain energy of δ-Ni_2Si is much less than that of NiAl. The addition of silicon promotes the nucleation and growth of δ-Ni_2Si, which depletes solute Ni in the copper matrix and thus retards the nucleation of the NiAl phase.

At early stage of aging, spinodal decomposition and $L1_2$ ordering attribute to the strength of the alloy. Increasing aging time and temperature, the precipitation hardening of Ni_3Al and δ-Ni_2Si is the main strengthening mechanism for the peak-aged alloy. According to Orowan strengthening mechanism, the increment of strength can be described as following [26]:

$$\Delta\sigma = \frac{0.81MGb}{2\pi(1-\nu)^{1/2}} \cdot \frac{\ln(d/b)}{(\lambda - d)} \quad (4)$$

$$\lambda = \frac{d}{2}\sqrt{\frac{2\pi}{3f}} \quad (5)$$

Here, $\Delta\sigma$ is the increment of strength; *M* is the Taylor-factor, which is 3.1 for copper; *G* is the shear modulus (45.5 GPa for Cu); *d* is the average diameter of precipitates; *b* is the Burgers vector (0.255

nm for Cu); ν is the Poisson's ratios (0.34 for Cu), λ is the average particle plane square lattice spacing; and f is the volume fraction of precipitates (assuming all the Ni formed Ni_2Si and Ni_3Al, the f should be 0.054%).

Obviously, the increment of strength increases with the decrease of average particle size and the increase of volume fraction. The addition of silicon strongly hindered the nucleation of large NiAl precipitates, so only continuous Ni_3Al and δ-Ni_2Si precipitation occurred. When the alloy was aged at 450 °C for 5 min, the particle size of precipitate was 3-4 nm but the volume fraction was low. Increasing aging time, the precipitates grew very slowly and the volume fraction increased, therefore, the Orowan strengthening caused by those precipitates increased with aging. When the alloy aged at 450 °C for 64 h, the particle Ni_3Al and δ-Ni_2Si precipitates was 15-20 nm, therefore the alloy showed high strength and hardness. Increasing aging temperature accelerated the precipitation process and the growth of precipitates. After aging at 550 °C for 120 min, the particle size of Ni_2Si and Ni_3Al was 15 nm and 25 nm, which were very effective in hindering the movement of dislocations and grain boundaries. Further increasing aging time or temperature, precipitates grew rapidly. Those large precipitates cannot effectively strengthen the alloy and the hardness decreased. Therefore, the alloy over-aged rapidly as temperature increased over 550 °C.

4. Conclusions

1) The phase transformation sequence of the solution treated Cu-10Ni-3Al-0.8Si alloy aged at 450 °C was that modulated structure and $L1_2$ ordering of matrix occurred, followed by continuous Ni_3Al ($L1_2$) precipitates and then continuous δ-Ni_2Si precipitates nucleated. At 550 °C, continuous Ni_3Al precipitated after 30 s, while δ-Ni_2Si and discontinuous precipitation occurred after 1 min. Increasing temperature to 650 °C, both continuous Ni_3Al and δ-Ni_2Si precipitated, and discontinuous precipitation occurred after aging for 30 s. At 750 °C, continuous Ni_3Al and δ-Ni_2Si formed after 30 s, and the metastable Ni_3Al was dissolved and cellular decomposition occurred after 15 min.
2) A large number of micro-twins formed in the matrix after the solution treated Cu-10Ni-3Al-0.8Si alloy was aged at 450 °C for 30 s, significantly improving the strength of the alloy.
3) The solution treated Cu-10Ni-3Al-0.8Si alloy showed excellent over-aging resistance at 450 °C, because of slow growth of the continuous Ni_3Al and δ-Ni_2Si precipitates and the strong inhibition of the nucleation of NiAl precipitates by the addition of silicon. When the aging temperature increased to above 550 °C, precipitates grew rapidly leading to the decrease of the hardness.

Acknowledgments

The work was supported by the National Natural Science Foundation of China (51271203), the Aid program for Science and Technology Innovative Research Teams in Higher Educational Institutions of Hunan Province, Hunan Provincial Natural Science Foundation (11JJ2025), Non-ferrous Metals Foundation of Hunan Province (YSZN2013CL06), Key Laboratory of Nonferrous Metallic Materials Science, Valuable Equipment Open Sharing Fund of Central South University (CSUZC201522).

References

[1] G.L. Xie, Q.S. Wang, X.J. M, B.Q. Xiong, L.J. Peng, J. Mater. Sci. Eng. A 558 (2012) 326-330.

[2] P. Scardi, M. Leoni, G. Straffelini, G. Giudici, J. Acta Mater. 55 (2007) 2531-2538.

[3] Y. Jin, N. Wei, J. Mech. Strength 19 (1997) 57-60.

[4] H. Zhang, Y.Z. Hui, X.M. Yuan, Y. Pan, J. Appl. Surf. Sci. 256 (2010) 5837-5842.

[5] R. Markandeya, S. Nagarjuna, D.S. Sarma, J. Mater. Charact. 54 (2005) 360-369.

[6] F. Mansfeld, H.H. Uhlig, J. Electrochem. Soc. 115 (1968) 900-904.

[7] L.N. Shen, Z. Li, Z.M. Zhang, Q.Y. Dong, Z. Xiao, Q. Lei, W.T. Qiu, Mater. Des. 64 (2014) 265-270.

[8] D.M. Zhao, Q.M. Dong, P. Liu, B.X. Kang, J.L. Huang, J. Mater. Chem. Phys. 79 (2003) 81-86.

[9] T. Hiroshi, I. Taichiro, N. Yutaka, J. Trans. Jim. 4 (1980) 431-435.

[10] Y.R. Cho, Y.H. Kim, T.D. Lee, J. Mater. Sci. 26 (1991) 2879-2886.

[11] M. Miki, Y. Amano, J. Trans. Jim. 20 (1979) 1-10.

[12] W.O. Alexander, D. Hanson, J. Inst. Met. 61 (1937) 275-291.

[13] H. Xie, L. Jia, Z. Lu, J. Mater. Charact. 60 (2009) 114-118.

[14] Q. Lei, Z. Li, C. Dai, J. Wang, X. Chen, J.M. Xie, W.W. Yang, D.L. Chen, Mater. Sci. Eng. A 572 (2013) 65-74.

[15] K.E. Amin, P.C. Becker, R.A. Piscitelli, J. Mater. Sci. Eng. A 49 (1981) 173-183.

[16] J. Wang, N. Li, O. Anderoglu, X. Zhang, A. Misra, J.Y. Huang, J.P. Hirth, J. Acta Mater. 58 (2010) 2262-2270.

[17] T. Hu, J.H. Chen, J.Z. Liu, Z.R. Liu, C.L. Wu, J. Acta Mater. 61 (2013) 1210-1219.

[18] A.R. Miedema, J. Phys. B 182 (1992) 1-17.

[19] A.R. Miedema, P.F. Chatel, F.R. Boer, J. Phys. B C 100 (1980) 1-28.

[20] C. Wolverton, V. Ozolin¸ s, M. Asta, J. Phys. Rev. B 69 (2004) 144109.

[21] J.D. Verhoeven, Wiley, New York, 1975, pp. 232-234.

[22] D. Watanabe, C. Watanabe, R. Monzen, J. Mater. Sci. 43 (2008) 3946-3953.

[23] M.J. Mehl, B.M. Klein, D.A. Papaconstantopoulos, Wiley, London, 1994, pp. 195-210.

[24] J.C. Zhao, M.R. Notis, J. Acta Mater. 46 (1998) 4203-4218.

[25] Z. Sierpi nski, J. Gryziecki, J. Mater. Sci. Eng. A 264 (1999) 279-285.

[26] M.X. Guo, K. Shen, M.P. Wang, Acta Mater. 57 (2009) 4568-4579.